ELSEVIER

Catalysis Today 38 (1997) 31–38

CATALYSIS TODAY

Gas transport in porous media under dynamic conditions

Pavel Čapek, Vladimír Hejtmánek, Olga Šolcová, Karel Klusáček*, Petr Schneider

Institute of Chemical Process Fundamentals, The Czech Academy of Sciences, Rozvojová 135, 165 02 Praha 6, Suchdol, Czech Republic

Abstract

The dynamic version of the Wicke–Kallenbach diffusion cell with one compartment closed and equipped with a sensitive pressure gauge was used for determination of sets of Mean Transport Pore Model and Dusty Gas Model parameters for an industrial catalyst (ICI 52-1 in reduced form). The dynamic pressure responses due to gas composition step changes of inert gases (H_2, He, N_2, Ar) were measured and fitted to the system of partial differential equations which describe the transport (mass balances with Maxwell–Stefan constitutive equations). The optimum textural parameters were obtained by simultaneous matching of all experiments. The model parameters are material constants of the porous solid and, thus, do not depend on temperature, pressure and kind of the transported gases. Both diffusion models gave a good agreement between experiments and calculations. The parameter reliability is discussed.

Keywords: Unsteady gas transport; Porous medium; Diffusion; Textural parameters

1. Introduction

The gas transport in porous media under unsteady conditions is quite common in practice. Start-up and switching off catalytic reactors, adsorption processes on porous adsorbents and random steady process fluctuations can be named as examples. The description of the dynamics of complex transport, adsorption and reaction steps as single and/or simultaneous processes is of basic importance for the process design and choice of optimum reactor and adsorber regimes.

The mass transport can only be isobaric when molar flux densities of mixture components, N_i, satisfy the generalised Graham law

$$\sum_{i=1}^{n} N_i (M_i)^{1/2} = 0, \qquad (1)$$

where M_i are molecular weights of components and n the number of components in the mixture. However, the mass transport inside the porous solids is generally non-isobaric because the ratios of fluxes are controlled by other conditions, e.g., the reaction stoichiometry or adsorption. Furthermore, the Graham law is violated under dynamic conditions even in the absence of reaction or adsorption. The pressure gradient which arises during unsteady transport of inert gases through porous solid can be used to evaluate parameters which describe the transport process. A suitable experimental technique which uses the dynamic version of the Wicke–Kallenbach diffusion cell with one compartment closed, developed by Novák et al. [1], is shown schematically in Fig. 1. The total pressure change in the bottom compartment of the cell which arises as a consequence of step change of gas composition in the upper cell compartment is followed and the pressure response

*Corresponding author. e-mail: klusacek@icpf.cas.cz

PII S0920-5861(97)00036-9

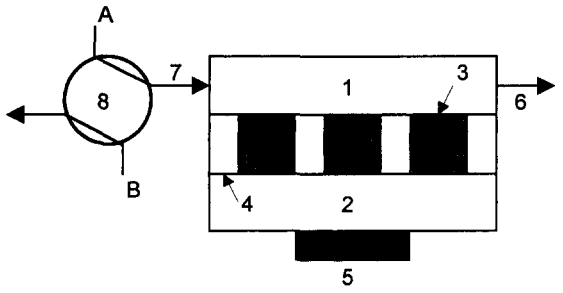

Fig. 1. Scheme of the cell. 1, upper compartment; 2, lower compartment; 3, porous pellets; 4, metallic disc; 5, membrane of pressure transducer; 6, cell outlet; 7, cell inlet; 8, 4-way valve.

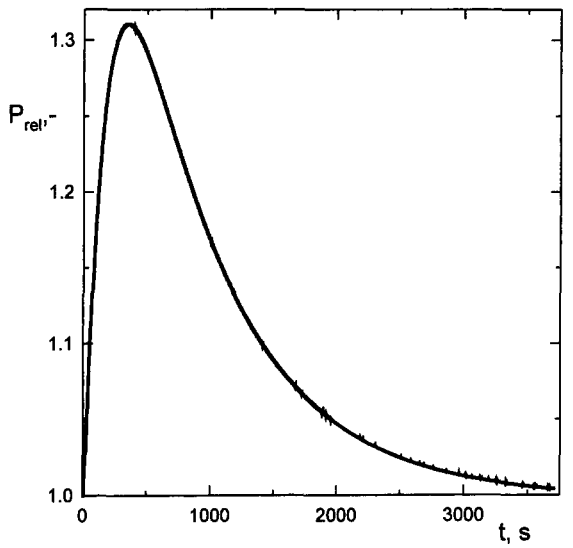

Fig. 2. Experimental pressure response for the step change $N_2 \rightarrow H_2$.

(see Fig. 2) is matched to the theoretical description.

Multicomponent mass transport in porous solids can be described both by the Mean Transport Pore Model or the Dusty Gas Model. The ability of both models to fit experimental data has been proven in literature. However, a little is known about the number of experiments needed to obtain good estimates of model parameters and about the influence of simultaneous matching of experiments with different inert gases. Similarly, comparison of both models based on a larger set of experiments has not been done up to now. It is the aim of this study to obtain (transport) parameters of the Mean Transport Pore Model and the Dusty Gas Model for an industrial catalyst ICI 52-1 in reduced form and to evaluate the confidence of these parameters estimated from a larger set of experiments.

2. Isothermal Maxwell–Stefan constitutive equations

The Dusty Gas Model (DGM) [2] and Mean Transport Pore Model (MTPM) [3] are based on the Maxwell–Stefan theory. Both models include contributions of bulk diffusion, Knudsen diffusion and permeation flow that accounts for both viscous flow and Knudsen flow. The vector form of the relation between molar flux densities, $\mathbf{N} = \{N_1, N_2 \ldots N_n\}^T$ and gradients of molar concentrations is the same for both models

$$\mathbf{H}(\mathbf{c}) \cdot \mathbf{N} + \frac{\partial \mathbf{c}}{\partial x} = 0, \tag{2}$$

where $\mathbf{c}$ is the vector of molar concentrations, $\mathbf{c} = \{c_1, c_2 \ldots c_n\}^T$ and $\mathbf{H}(\mathbf{c})$ is a square $(n \times n)$ concentration dependent matrix (for matrix elements, h_{ij}, see Appendix A). This matrix does not show [1] the differences between both models. The matrix elements depend on transport properties of pure gases and their binary mixtures, and on the structure of the porous solid. The pore structure is characterised by three parameters which are related (i) to effective porosity of transport pores, ψ; (ii) to the mean transport pore radius, $\langle r \rangle$; (iii) and to the mean of the square of transport pore radii (MTPM) or to the coefficient of the viscous flow (DGM), $\langle r^2 \rangle$. These parameters represent porous solid material properties related to mass transport and, thus, do not depend on temperature, pressure and the kind of gases transported. They have to be determined experimentally, preferentially with inert gases.

3. Experimental

Experiments were performed in the diffusion cell, shown in Fig. 1, at laboratory temperature and atmospheric pressure. The cell consists of two compartments separated by a metallic disc. The cylindrical pellets of an industrial porous catalyst ICI 52-1 (for properties see Table 1) were mounted, in parallel, in cylindrical holes of the metal disc; thus, only the

Table 1
Diffusion cell and pellet data

Inlet volumetric flow rate, F^0 (cm^3/s)	1.34
Upper compartment volume, V_L (cm^3)	19.1
Lower compartment volume, V_0 (cm^3)	55.2
Pellet height (cm)	0.368
Pellet diameter (cm)	0.540
Number of pellets	12
Pellet total porosity (ε)	0.623

circular pellet faces are open for one-dimensional transport of gases. The inlet to the upper compartment of the diffusion cell is connected to a four-way valve which permits swapping the gas stream entering in the cell by another gas stream. The flow rates are controlled by mass flow meter-controllers. The closed lower compartment is equipped with a sensitive pressure gauge. The time development of the gauge response after the inlet composition change ($t = 0$) is logged with frequency 1 Hz in a computer. Before the start of the run, the cell is flushed with gas A (e.g., nitrogen). At the start of the run, gas A was replaced by another gas B (e.g., helium). The composition step change at the inlet of the upper compartment is denoted as A → B (e.g., N_2 → He). The system response for the case $N_2 \rightarrow H_2$ is shown in Fig. 2.

Table 2
List of experiments. Parentheses mark binary mixtures (1 : 1)

Run	Composition at the inlet of upper compartment		Maximum/minimum pressure in lower compartment	
(-)	$t < 0$	$t \geq 0$	t (s)	P_{rel} (-)
1	N_2	H_2	352	1.310
2	H_2	N_2	372	0.660
3	He	N_2	430	0.732
4	N_2	He	435	1.244
5	Ar	He	450	1.295
6	He	Ar	479	0.679
7	H_2	Ar	422	0.609
8	Ar	H_2	379	1.360
9	(H_2,Ar)	He	557	1.123
10	(He,Ar)	H_2	340	1.222
11	H_2	(He,Ar)	371	0.754
12	(H_2,N_2)	Ar	446	0.803
13	Ar	(H_2,N_2)	421	1.183
14	(He,N_2)	Ar	516	0.822
15	Ar	(He,N_2)	485	1.163

3.1. Gases

Hydrogen, helium, nitrogen and argon, which do not adsorb on the catalyst ICI 52-1, were used as test gases. The step changes performed using pure gases and gas mixtures are listed in Table 2 which summarises also the co-ordinates of the response extremes.

3.2. Porous pellets

The fresh catalyst was reduced [4] at 200°C by 5% hydrogen in helium and cooled down under helium flow. The reduced catalyst was passivated by slow admission of air. The passivated catalyst pellets were fixed in the cylindrical holes of the metallic disc by silicon–rubber tubing.

4. Mass balance of diffusion cell

Mass balances for n gas mixture component inside the porous pellets supplement the constitutive Eq. (2)

$$\varepsilon \frac{\partial \mathbf{c}(t,x)}{\partial t} = -\frac{\partial \mathbf{N}(t,x)}{\partial x}, \tag{3}$$

where ε is the pellet porosity and t the time. Boundary conditions of the system of partial differential Eqs. (2) and (3) follow from the mass balance of both compartments assuming no resistance to mass transport between the bulk gas and the pellet.

If ideal mixing is assumed at $x = 0$ (lower compartment), the condition has the form

$$V_0 \frac{\partial \mathbf{c}(t,0)}{\partial t} = -\frac{V_p}{L}\mathbf{N}(t,0), \tag{4}$$

where V_0 is the free volume of the compartment, V_p the (geometric) volume of cylindrical pellets in the metallic disc and L their length.

At $x = L$ (upper compartment) the boundary conditions are

$$V_L \frac{\partial \mathbf{c}(t,L)}{\partial t} = F^0\mathbf{c}^0 - FBOL@\mathrm{c}(t,L) + \frac{V_p}{L}\mathbf{N}(t,L), \tag{5}$$

where F^0 and F are the volumetric flow gas rates at the compartment inlet and outlet, respectively, and V_L is the compartment volume. Eq. (5) again assumes ideal

mixing in the compartment. The unknown outlet volumetric flow rate, F, in Eq. (5) is obtained from the overall mass balance

$$F = F^0 + \frac{V_p}{Lc_T}\sum_{i=1}^{n} N_i(t, L), \tag{6}$$

where c_T is the total molar gas concentration, a constant.

Initial conditions for the system Eqs. (2)–(6) are formulated as

$$\mathbf{c}(0, x) = \mathbf{c}^*$$

with the vector of constant component concentrations, $\mathbf{c}^* = \{c_1^*, c_2^* \ldots c_n^*\}^T$, determining the equilibrium state when the cell is completely flushed by a single gas or gas mixture.

The system of Eqs. (2)–(6) was integrated by method of lines [5]. The discretization of the integral form of Eq. (3) was achieved [6] by dividing the pellet into small volume elements (up to 50). The resulting system of ordinary differential equations was solved using backward differentiation formulas [7].

5. Optimisation

The transport parameters were obtained by minimisation of an objective function which considered two aspects: (a) both models predict that transport parameters do not depend on the kind of gases used, i.e., the same parameters should result from matching individual runs; (b) because of the possible experimental error and parameter correlation all experiments were matched simultaneously. The objective function, χ^2, was defined as weighted sum of squares of deviations between calculated relative pressures, $P(t)$, calculated as (Eq. (4))

$$P(t) = \sum_{i=1}^{n} c_i(t, 0)/c_T \tag{7}$$

and experimentally determined relative pressures, $P^{exp}(t)$, in the lower cell compartment

$$\chi^2(\psi, \langle r\rangle, \langle r^2\rangle) = \frac{1}{m}\sum_{j=1}^{m}\frac{1}{s_j}\sum_{i=1}^{s_j}\left(P_{i,j}^{exp}(t) - P_{i,j}(t)\right)^2 \tag{8}$$

where s_j is the number of pairs $t - P(t)$ in the jth experimental run and m the number of experimental runs. The weighted sum of the squares was chosen because of different lengths of runs. Thus, longer runs with heavier gas pairs are not more heavily weighted than runs with lighter gas pairs.

The objective function (8) was minimised by the simplex algorithm of Nelder and Mead [8]. To save time, the integration was performed with low accuracy in the spatial variable at the start of the optimisation. Near the optimum the accuracy of integration was improved by increasing the number of grid points. In order to avoid local minima the optimisation was restarted with different initial parameter guesses and a different simplex sizes. Constrains based on physical considerations and results of the mercury porosimetry were applied, i.e., ψ, must be within $(0, \varepsilon, \langle r\rangle \geq 1$ nm and $\langle r^2\rangle \geq 10$ nm^2.

6. Results and discussion

The obtained DGM and MTPM transport parameters are summarised in Table 3. In addition to the simultaneous matching of all ($m = 15$) experimental runs, transport parameters were also determined by matching of pairs of runs and all binary and ternary runs. This should supply information about parameter confidence and the amount of information held by each experimental run.

6.1. DGM

Transport parameters ψ and $\langle r\rangle$ estimated from pairs of binary runs do not differ significantly. By simultaneous matching of all binary runs (runs 1-8) similar values of the first two parameters, ψ and $\langle r\rangle$, are obtained (cf. Table 3). Determination of transport parameters from a single ternary run (run 9) and from pairs of ternary runs (runs 10–15) was difficult. Both transport parameters were loaded with large uncertainty. The large deviation of transport parameters obtained from runs 10 and 11 (in which a mixture of Ar with a light gas is replaced by a light gas) is difficult to explain. An interesting behaviour was observed when all ternary runs were included in parameter estimation: transport parameters were close to the final values (the last row in Table 3). The highest

Table 3
Optimum DGM and MTPM parameters. For run numbers see Table 2.

Runs	DGM				MTPM			
	ψ (-)	$\langle r\rangle$ (nm)	$\langle r^2\rangle$ (nm^2)	$10^4\,\chi^2$ (-)	ψ (-)	$\langle r\rangle$ (nm)	$\langle r^2\rangle$ (nm^2)	$10^4\,\chi^2$ (-)
1,2	0.0644	58.6	9750	0.166	0.0774	48.0	8400	0.142
3,4	0.0580	71.8	4680	0.295	0.0638	65.1	4150	0.269
5,6	0.0582	70.3	5120	0.291	0.0663	61.5	4360	0.216
7,8	0.0564	71.4	7170	0.173	0.0757	50.42	6910	0.199
9	0.0678	55.2	6720	0.399	0.0888	40.9	6710	0.387
10,11	0.240	11.7	5440	0.171	0.234	12.1	5450	0.184
12,13	0.0432	117.2	10	0.210	0.0519	95.5	10	0.129
14,15	0.0538	86.7	10	0.268	0.0593	77.7	10	0.168
1–8	0.0602	65.8	7450	0.304	0.0721	54.1	6560	0.268
9–15	0.0910	36.1	9590	0.756	0.109	29.6	8230	0.751
1–15	0.0687	53.5	9340	0.386	0.0795	46.0	7990	0.347

uncertainty was found for the third transport parameter, $\langle r^2\rangle$. For some runs (runs 12, 13, 14 and 15) $\langle r^2\rangle < 10$ nm^2, i.e., below the threshold value. Nevertheless, simultaneous matching of all binary and ternary runs provides a good estimate of $\langle r^2\rangle$ (cf., the last two rows of Table 3).

6.2. MTPM

MTPM transport parameters were determined in a slightly different way than DGM. This model includes contributions of Knudsen flow and viscous slip on the capillary wall. It predicts different permeability coefficients, B_i, for each component unlike DGM. We used the simplified relation for the permeability coefficient

$$B_i = D_i^{\mathrm{k}}\frac{\omega + K_i}{1 + K_i} + \frac{\psi\langle r^2\rangle p}{8\mu}, \quad i = 1\ldots n \tag{9}$$

because its original more complex version [3] caused serious troubles during optimisation: the optimum transport parameters were often unrealistic ($\psi \to 0$, $\langle r\rangle \to 1$ nm, $\langle r^2\rangle \to 0$ nm^2). In Eq. (9), K_i is the Knudsen number, μ the mixture viscosity, p the total pressure and D_i^{k} the effective Knudsen diffusion coefficient. The Knudsen number is dependent on the mixture composition and the total pressure [3] while the mixture viscosity under a low pressure depends only on the mixture composition. The value of a numeric slip constant, ω, proposed in literature lies in the interval 0.6–1.4. Therefore, as the first step, minimisation was performed for a series of slip constant from the above interval with step 0.1. This was done in order to keep the same number of optimised parameters for both MTPM and DGM. The lowest value of the objective function, χ^2, found for $\omega = 1.4$ was only slightly worse than for $\omega = 1$. As shown in Table 4 the slip parameter strongly influences the other transport parameters but there is no significant improvement of χ^2. With increase of ω the geometric parameter, ψ, increases and parameters $\langle r\rangle$ and $\langle r^2\rangle$ decrease. The slip of molecules at the wall is only one of the several mass transport mechanisms accounted for by MTPM and, perhaps, experimental runs do not contain sufficient information to estimate ω. Therefore, $\omega = 1$ was assumed and in the second optimisation step the simplified form of Eq. (9) was used

Table 4
Influence of the slip constant on MTPM transport parameters

ω (-)	ψ (-)	$\langle r\rangle$ (nm)	$\langle r^2\rangle$ (nm^2)	$10^4\,\chi^2$ (-)
0.6	0.0530	83.8	17200	0.506
0.7	0.0603	68.4	14000	0.441
0.8	0.0657	60.2	11500	0.397
0.9	0.0727	52.1	9500	0.367
1.0	0.0795	46.0	8000	0.347
1.1	0.0792	46.2	7950	0.347
1.2	0.0872	40.8	6730	0.333
1.3	0.104	32.6	5000	0.317
1.4	0.112	29.5	4400	0.312

$$B_i = D_i^{\mathrm{k}} + \psi\langle r^2\rangle p/(8\mu), \quad i = 1\ldots n \tag{10}$$

Additional experiments with pure gases in the cell [9] could bring a missing information on the slip constant.

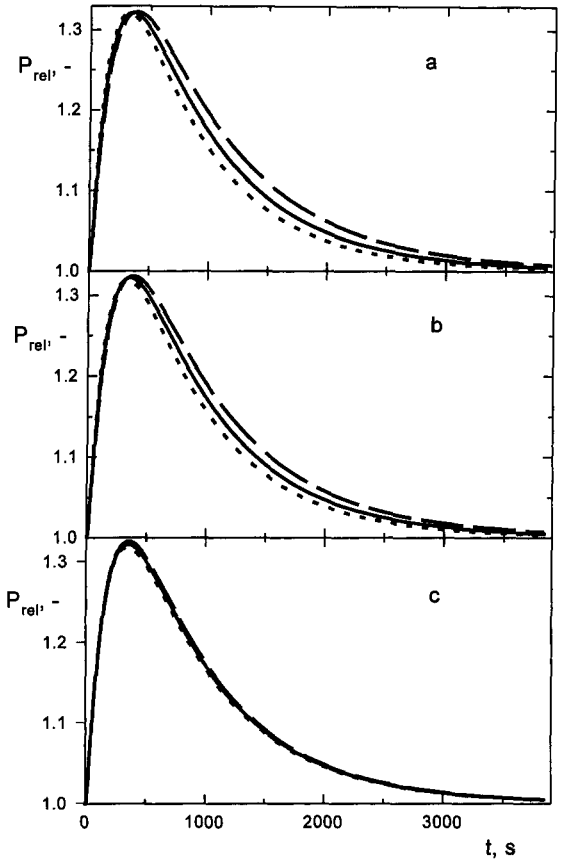

Fig. 3. DGM parameter sensitivity, (a) ψ, (b) $\langle r \rangle$, (c) $\langle r^2 \rangle$, for step change $N_2 \rightarrow H_2$. Full lines calculated for optimum parameters, dashed lines for 0.9 times optimum parameters and dotted lines for 1.1 times optimum parameters.

6.3. Comparison of MTPM and DGM

There is no major difference between the optimum MTPM and DGM transport parameters and between the corresponding objective functions (Table 3).

The higher uncertainty of the third parameter, $\langle r^2 \rangle$, can be explained by the small mean transport pore radius, $\langle r \rangle$. In such narrow pores the viscous flow is of less importance and, consequently, $\langle r^2 \rangle$ can not be estimated too reliably. This is in agreement with the parameter sensitivity determined for the step change $N_2 \rightarrow H_2$. Perturbation of the optimum DGM transport parameters ψ and $\langle r \rangle$ influences the time dependence of pressure in the lower cell compartment (Fig. 3a,b). The change of $\langle r^2 \rangle$, however, does not alter the response significantly (Fig. 3c). For MTPM similar behaviour was found.

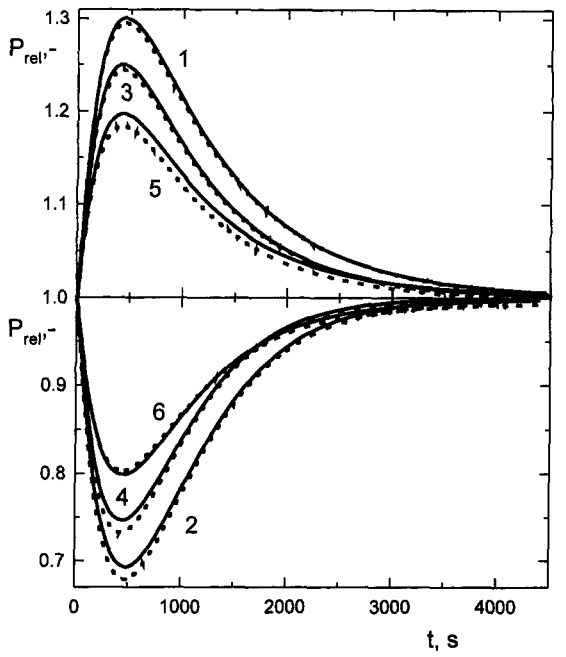

Fig. 4. Comparison of experimental (●●●●) and calculated (————) pressure responses for DGM. Step changes: 1, Ar → He; 2, He → Ar; 3, N_2 → He; 4, He → N_2; 5, Ar → (H_2,N_2); 6, (H_2,N_2) → Ar.

Experimental cell responses are compared with simulations based on optimum MTPM and DGM parameters as shown in Figs. 4 and 5. As can be seen, both models fit the experimental curves well. In agreement with the similarity of χ^2 for both models, no model can be classified as superior.

The experiments with binary combinations of four different gases and the simultaneous matching of experimental runs proved to be sufficient for obtaining reliable transport parameters. The experiments with ternary gas mixtures have shown that the underlying theory is capable of correctly predicting the transport of multicomponent gas mixtures.

7. Conclusions

The transport parameters of MTPM and DGM for the reduced catalyst ICI 52-1 were determined by simultaneous matching of experimental responses.

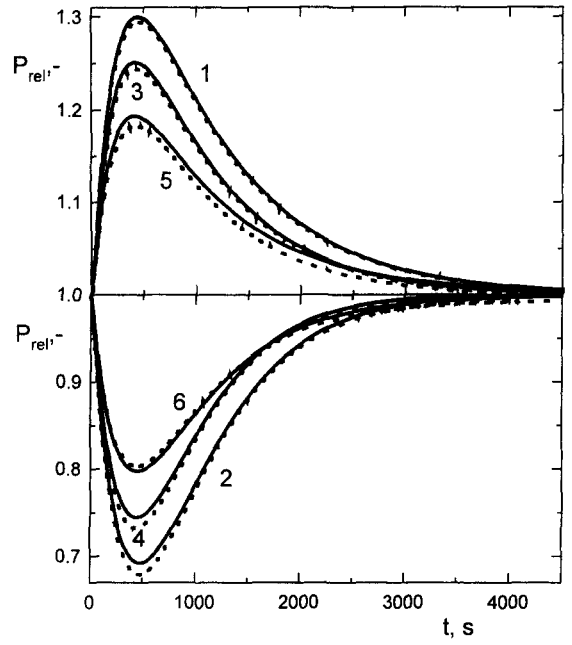

Fig. 5. Comparison of experimental (●●●●) and calculated (———) pressure responses for MTPM. Step changes: 1, Ar → He; 2, He → Ar; 3, N_2 → He; 4, He → N_2; 5, Ar → (H_2, N_2); 6, (H_2, N_2) → Ar.

These models correctly describe the combined multicomponent gas transport in a porous solid. The transport parameter reliability was discussed in order to find the appropriate amount of experimental information needed for parameter estimation.

8. Notation

8.1. Symbols

B_i	effective permeability coefficient
c	vector of molar concentrations
c_i	molar concentration
c_T	total molar concentration in the upper compartment
D_i^k	effective Knudsen diffusion coefficient
D_{ij}	effective bulk diffusion coefficient of pair *i-j*
F	volumetric flow rate
H(c)	$n \times n$ matrix
h_{ij}	elements of matrix **H(c)**
K_i	Knudsen number
L	pellet length
M_i	molecular weight
m	number of experimental runs
N	vector of molar flux densities
N_i	molar flux density
n	number of components in the gas mixture
$P(t)$	relative total pressure in lower compartment
p	total local pressure
R_g	gas constant
$\langle r \rangle$	mean pore radius
$\langle r^2 \rangle$	mean of squares of transport pore radii
s_j	number of pairs $t - P(t)$ in one experimental run
T	thermodynamic temperature
t	time
V_0	volume of lower compartment
V_L	volume of upper compartment
V_p	volume of all pellets
x	spatial variable

8.2. Greek letters

ε	total pellet porosity
μ	mixture viscosity
χ^2	objective function
ψ	geometric constant of porous solid
ω	slip constant

8.3. Superscript

0	cell inlet

Acknowledgements

The financial support by the Volkswagen Foundation, Hannover, FRG (grant # I/69084) and the Grant Agency of the Czech Republic (grant # 104/94/1025) is gratefully acknowledged.

Appendix A

The elements of matrix **H(c)** are defined as

$$h_{ij} = 1/D_i^k + (c_i\alpha_i/D_i^k) + \sum_{k=1}^{n}(c_k/c_T D_{ik})$$

$$h_{ij} = c_i\alpha_i/D_j^k - c_i/(c_T D_{ij}) \quad i \neq j,$$

where D_{ij} is the effective bulk binary diffusion

coefficient defined as $D_{ij} = \psi \boldsymbol{D}_{ij}$ and D_i^{k} is the effective Knudsen diffusion coefficient

$$D_i^k = \psi 2/3\langle r\rangle \sqrt{8R_{\mathrm{g}}T/(\pi M_i)}.$$

The bulk binary diffusion coefficients, D_{ij}, were taken from Marrero and Mason [10]. Differences between MTPM and DGM appear in the definition of parameter α_i:

for MTPM

$$\alpha_i = \left(1 - B_i/D_i^{\mathrm{k}} - \sum_{k=1}^{n} c_k(B_i - B_k)/c_{\mathrm{T}}D_{ik}\right) \Bigg/ \times \sum_{k=1}^{n} c_k B_k/D_k^{\mathrm{k}},$$

for DGM

$$\alpha_i = -(\beta/D_i^{\mathrm{k}}) \Bigg/ \left(\sum_{k=1}^{n} c_k + \beta \sum_{k=1}^{n} c_k \Big/ D_k^{\mathrm{k}}\right)$$

$$\beta = \psi\langle r^2\rangle p/(8\mu).$$

The mixture viscosity in the latest formula depends on the mixture composition.

The mixture viscosity, μ, used in MTPM (Eqs. (9) and (10)) and DGM was determined by the Reichenberg's formula [11].

References

[1] M. Novák, K. Ehrhardt, K. Klusácek and P. Schneider, Chem. Eng. Sci., 43 (1988) 185.
[2] E.A. Mason and A.P. Malinauskas, Gas Transport in Porous Media: The Dusty Gas Model, Elsevier, Amsterdam, 1983.
[3] P. Schneider, Chem. Eng. Sci., 33 (1978) 1311.
[4] P. Capek and K. Klusacek, Chem. Eng. Sci., 49 (1994) 4095.
[5] R.F. Sincovec and N.K. Madsen, ACM Trans. Math. Software, 1 (1975) 261.
[6] K. Ehrhardt, K. Klusacek and P. Schneider, Comput. Chem. Eng., 12 (1988) 1151.
[7] A.C. Hindmarsh, ODEPACK, A Systematized Collection of ODE Solvers, in Scientific Computing, R.S. Stepleman et al. (Eds.), North-Holland, Amsterdam, 1983, p. 55-64.
[8] D.M. Himmelblau, Nonlinear Programming, McGraw-Hill, New York, NY, 1972, p. 148..
[9] P. Fott and G. Petrini, Appl. Catal., 2 (1982) 367.
[10] T.R. Marrero and E.A. Mason, J. Phys. Chem. Ref. Data, 1 (1972) 3.
[11] R.C. Reid, J.M. Prausnitz and B.E. Poling, The properties of Gases and Liquids, McGraw-Hill, New York, NY, 1988, p. 404.